Soft Matter

Accepted Manuscript

ROYAL SOCIETY OF CHEMISTRY

rsc.li/soft-matter-journal

View Article Online
DOI: 10.1039/D5SM01244A

Soft Matter

ARTICLE TYPE

Cite this: DOI: 00.0000/xxxxxxxxxx

Skyrmionic topology perspective on Lehmann clusters

Pawel Pieranski[a], Ivan Smalyukh[b,c], Mehdi Zeghal[a], Patrick Judeinstein[d] and Maria Helena Godinho[e]

Received Date
Accepted Date

DOI: 00.0000/xxxxxxxxxx

When two parallel coplanar dislocations with opposite Burgers vectors are brought by action of a stress into a collision in solid crystals, they annihilate each other. In cholesterics with the pitch p, in certain conditions, colliding dislocations with Burgers vectors b=p and b=-p are immune against annihilation and form stable twin-like pairs known as Lehmann clusters. We point out that this immunity is due to the escape into the third dimension of the director field. We show that from topological point of view the Lehmann clusters can be seen as skyrmion tubes embedded in a helicoidal background and their extremities have topology of monopoles.

[

1 Collisions of parallel coplanar dislocation

1.1 Annihilation of dislocation pairs in solid crystals

In solid crystals, two parallel coplanar dislocations with opposite Burgers vectors, brought by action of a stress into a collision, annihilate each other as it is shown schematically in Figure 1.

1.2 Lehmann clusters: twin-like pairs of cholesteric dislocations immune against annihilation

Experiments of Smalyukh and Lavrentovich (S&L) with cholesterics confined between surfaces with planar anchorings[1] have shown that in certain conditions, two parallel coplanar dislocations can be immune against annihilation and form stable twin-like pairs. Using Confocal Polarizing Fluorescence Microscopy, S&L have found that such stable pairs are composed of dislocations with opposite Burgers vectors $b = p$ and, $b = -p$, where p is the cholesteric pitch (see Figs. 2, 3, 4 and 6).

Inspired by the pioneer work of Kleman and Friedel[2], S&L proposed models for the director field of stable pairs. As shown in Figure 3 , they consist of sets of four disclinations $\{\lambda^{+1/2}, \lambda^{-1/2}, \lambda^{-1/2}, \lambda^{+1/2}\}$ or $\{\tau^{+1/2}, \tau^{-1/2}, \tau^{-1/2}, \tau^{+1/2}\}$ located at vertices of a rhombus. Knowing that such clusters of four disclinations were observed already by Otto Lehmann[3,4], S&L proposed to call the stable pairs of dislocation - "Lehmann clusters".

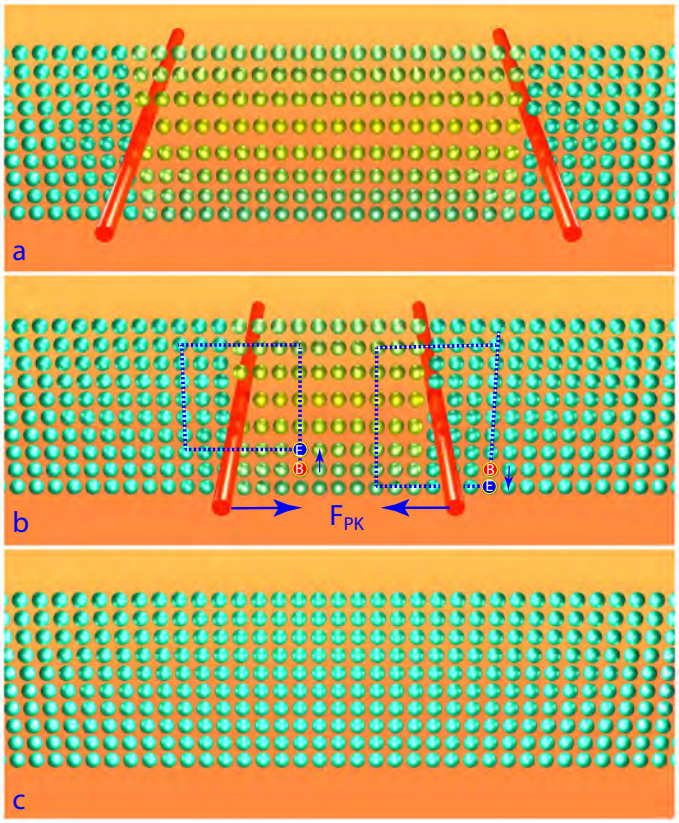

Figure 1 Annihilation of a pair of parallel coplanar edge dislocations with opposite Burgers vectors in a solid crystal.

[a] Laboratoire de Physique des Solides, Université Paris-Saclay, 91405 Orsay, France.
[b] Department of Physics, University of Colorado, Boulder, CO 80309-0390, USA.
[c] International Institute for Sustainability with Knotted Chiral Meta Matter (WPI-SKCM[2]), 2-313 Kagamiyama, Higashi-Hiroshima City, Hiroshima, Japan.
[d] Université Paris-Saclay, CEA, CNRS, LLB, 91191 Gif-sur-Yvette, France.
[e] i3N/CENIMAT, Department of Materials Science, NOVA School of Science and Technology, NOVA University Lisbon, Campus de Caparica, Caparica 2829 - 516, Portugal.
* corresponding author, Email: pawel.pieranski@universite-paris-saclay.fr

View Article Online
DOI: 10.1039/D5SM01244A

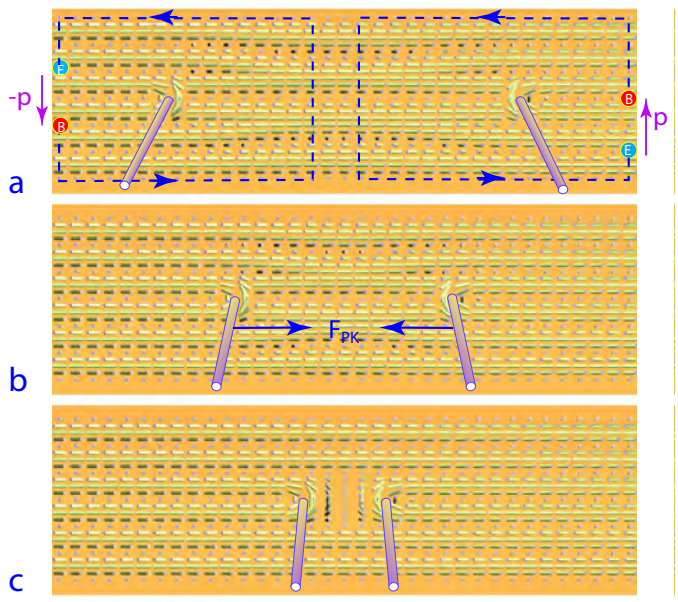

Figure 2 Pair of dislocations with opposite Burgers vectors vectors $b = p$ and $b - p$ in a cholesteric layer. Upon a collision driven by the Peach-Koehler force F_{PK}, they do not annihilate but form a stable twin-like pair known as Lehmann cluster.

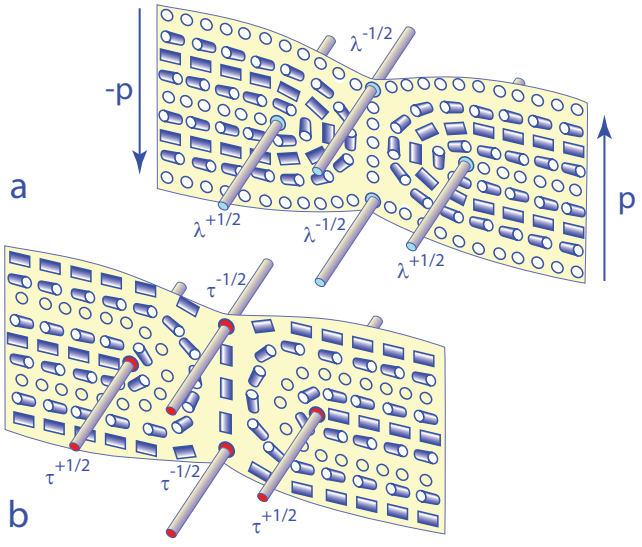

Figure 3 Models of the director field of the Lehman cluster proposed by Smalyukh and Lavrentovich[1]: a) four non-singular disclinations λ, b) four singular disclinations τ.

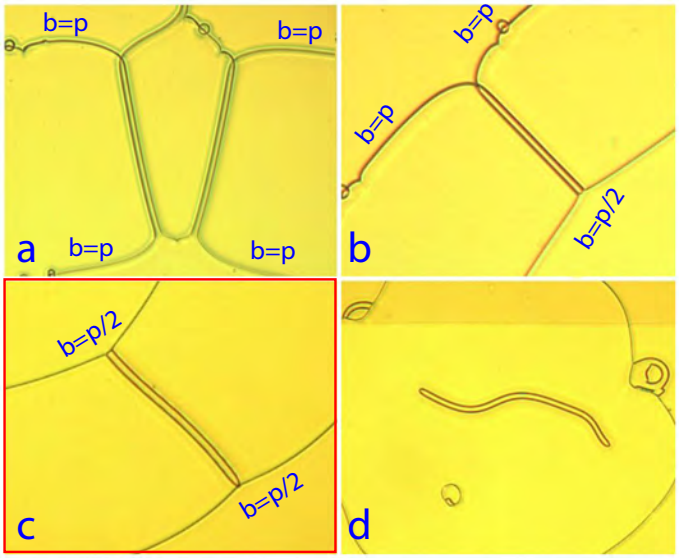

Figure 4 Occurrence of Lehmann clusters. a) As crossings of $b = p$ dislocations. b) Spanned between the $b = p$ and $b = p/2$ dislocations. c) Spanned between two $b = p/2$ dislocations. This type of Lehmann clusters is considered in details in this paper. d) As a closed worm-like loop equivalent to a skyrmion tube (see Section 6.2).

1.3 Role of the Lehmann clusters in stability of tangles, knots and links

Since the generic work of Smalyukh and Lavrentovich[1], twin-like pairs of dislocations immune against annihilation were also observed in experiments with tangles[5], knots[6] and links[7,8] made of cholesteric dislocations with the Burgers vector b equal to the full (2π) pitch p. Crossings in such knots and links have frequently the structure of Lehmann clusters. Therefore the immunity of tangles, knots and links against the rewiring is similar to that of the Lehmann clusters discussed here.

1.4 Occurrence of Lehmann clusters

The occurrence of Lehmann clusters in patterns of dislocations in cholesterics confined in gaps of variable thickness is summarized in Figure 4 and can be classified into four types (see also the S&L article[1]):

Type 1 : They can appear as crossings between $b = p$ dislocations (see Figure 4a).

Type 2 : They can be spanned between $b = p$ and $b = p/2$ dislocations (see Figure 4b).

Type 3 : They can be spanned between two $b = p/2$ dislocations (see Figure 4c). This paper is devoted to this type of Lehmann clusters.

Type 4 : They can be independent. In this case, they form a worm-like narrow loops (see Figure 4d) and are not stable because the length of such loops decreases in time until the final collapse occurs.

View Article Online
DOI: 10.1039/D5SM01244A

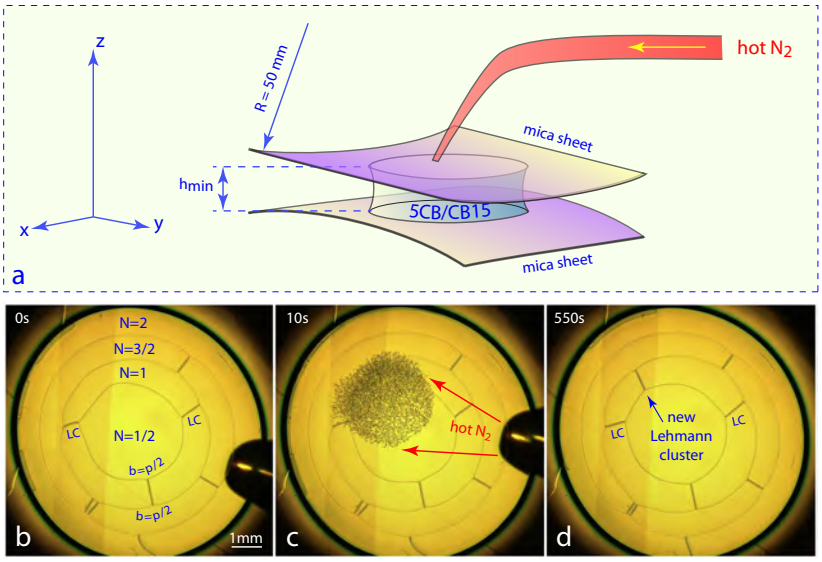

Figure 5 Controlled generation of Lehmann clusters. a) Experimental setup. b) Eight Lehmann clusters spanned between circular $b = p/2$ dislocations loops. N is the number of full cholesteric pitches located between the mica sheets. c) Dense skein of dislocations generated locally by the sequence of phase transitions: cholesteric $\rightarrow$ isotropic $\rightarrow$ cholesteric. d) After relaxation, a new Lehmann cluster appears. Like the initial eight ones, it is spanned between two $b = p/2$ loops. (see videos S1 and S2 of Supplementary Information)

1.5 Aims of this paper

In the present paper we will explain the immunity of the Lehmann clusters against annihilation (or rewiring) in terms of an alternative, singularity-free solitonic model of the director field resulting from the escape into the third dimension.

Before these theoretical considerations in section 3, we will report in the next section 2 on new experiments focussed on a controlled generation of Lehmann clusters of the type 4.

2 Experimental

2.1 Haphazard occurrence of Lehmann clusters

It is well known that cholesterics confined in gaps of variable thickness contain dislocation patterns made of $b = p/2$ and $b = p$ dislocations. In the sphere/plane geometry, the ground state is composed of separated concentric circular dislocation loops. In practice, this ideal ground state configuration is rather rare because after their preparation, involving flows and/or isotropic $\rightarrow$ cholesteric transition, the cholesteric droplets contain dense skeins of knotted and linked dislocations that decay slowly by rewiring of crossings. On long time scale, the decay process leads to metastable patterns of interconnected loops.

Most frequently, the circular loops are interconnected by crossings such as those in Figure 4a so that the dislocation patterns can contain knots or links. Connections of the $b = p/2$ dislocation loops by Lehmann clusters (Figure 4c) can exist as well but beside the generic work of S&L[1], little attention was payed to them.

Obviously, the production of Lehmann clusters by the decay of random skeins of dislocations is haphazard. The setup described below was tailored for a more efficient production of Lehmann clusters.

2.2 Setup

The setup represented in Figure 5a is a modified version of the one used previously in experiments with tangles[5], knots[6,9] and links[7].

It consists of two mica sheets, supported and bent into cylindrical shapes by plastic parts described in details previously[6,8]. The small vertical distance h_{min} between the mica sheets is controlled with accuracy of $0.5\mu m$ by means of a micrometric translation stage[6,8]. The cholesteric sample - a droplet of the 5CB/CB15 mixure (see Section 3 of Supplementary Information) - is confined by capillarity inside the gap between the mica sheets.

With the aim to melt the cholesteric sample into the isotropic phase, the setup was modified by addition of a system blowing a jet of hot nitrogen gas ($T \approx 40^oC$) on the upper mica sheet through a conical nozzle (a micro-pipette tip) as shown in Figure 5a.

After the melting of the sample into the isotropic phase, the hot nitrogen jet is switched off and the cholesteric phase is recovered by spontaneous cooling at ambient temperature ($T \approx 20^oC$). Due to the very small thicknesses of the mica sheets and of the cholesteric droplet ($\approx 100\mu m$), the characteristic times of heating and cooling are of the order of magnitude $\approx 1s$. The size of the area heated by the hot gas depends on the vertical distance between the pipette tip and the upper mica sheet. Typically, its diameter is of the order of $2mm$.

2.3 Generation of Lehmann clusters

In the experiment represented in Figs. 5b-d, the cholesteric droplet contains initially (see Figs. 5b) three circular concentric $b = p/2$ dislocation loops interconnected already by seven Lehmann clusters. The $b = p/2$ loops separate fields labeled with indices N corresponding to the number of full cholesteric pitches

View Article Online
DOI: 10.1039/D5SM01244A

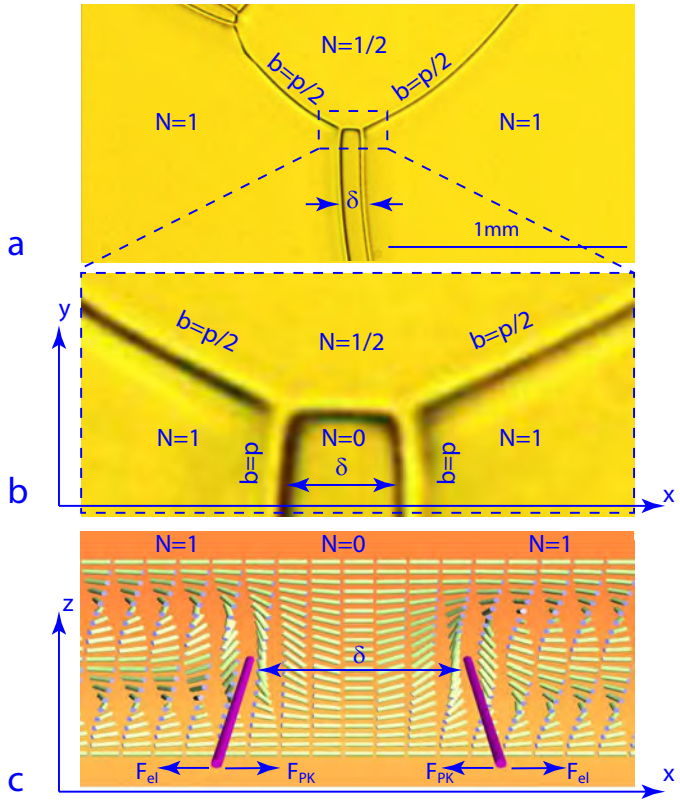

Figure 6 Structure of Lehmann clusters. a) Junction between a Lehmann cluster and a $p/2$ dislocation loop. b) Close-up of the junction. c) Defect-free variant of the director field in the (x,z) cross section of the Lehmann cluster (see section 3).

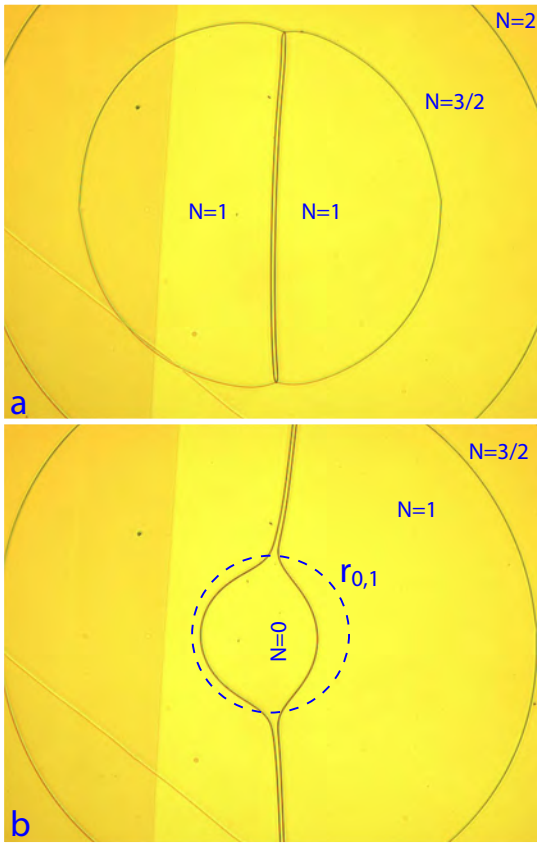

Figure 7 Splitting of the Lehmann cluster upon reduction of the thickness h_{min}. a) $h_{min} > p_o/2$. b) $h_{min} < p_o/2$. (see Video 4 of Supplementary Information)

located between the mica sheets.

This initial pattern is heated locally and shortly by the hot nitrogen jet. The size of the area in which the cholesteric $\rightarrow$ isotropic melting occurred is the order of $2mm$. After cooling back into the cholesteric phase, this area contains a dense skeins of dislocations (see Figure 5c). The elastic relaxation of this skeins lasts about $550s$ and leads to formation of a new Lehmann cluster visible in Figure 5d. **Remark**: generation of a Lehmann cluster by just one sequence of cholesteric $\rightarrow$ isotropic $\rightarrow$ cholesteric phase transitions is not granted. In practice, the experiment must be repeated several times until the new Lehmann cluster is created.

2.4 Structure of Lehmann clusters

In the simplest case, the Lehmann cluster has the structure depicted in Figure 6. It is spanned inside the annular field labeled as N between two circular $b = p/2$ dislocations. One of them is visible in Figs. 6a and 6b. The second one, separating fields with $N = 1$ and $N = 3/2$ pitches, is located outside of the area visible in Figure 6a.

This Lehmann cluster itself is made of a pair of $b = p$ and $b = -p$ parallel dislocations separating fields with $N = 1$ and $N = 0$ cholesteric pitches (see Figure 6b). The two dislocation are pushed one against the other by Peach-Koehler forces F_{PK} determined by the local thickness as discussed below. The equilibrium distance δ between them is determined by the balance between this Peach-Koehler force F_{PK} and the force F_{el} of the repulsive elastic interaction which grows with the inverse of the distance δ between the dislocations.

Independently of quantitative details concerning the equilibrium distance δ, we will point out in section 3 that δ cannot tend to zero because the pair of dislocation of this Lehmann cluster is protected topologically against annihilation.

2.5 Splitting of the Lehmann cluster

Let us consider the experiment represented in Figure 7 where a Lehmann cluster is spanned inside the central $b = p/2$ loop. This experiment shows that the Lehmann cluster is stable as long as the minimal thickness h_{min} between the cylindrical mica sheets is larger than $p_o/2$ where p_o is the equilibrium cholesteric pitch which is the case in the Figure 7a. By the way, let us note that the stability of the central dislocation loop depends also on the minimal thickness h_{min}; for $h_{min} > 3p_o/4$ it collapses.

Upon reduction of the minimal thickness h_{min} below $p_o/2$, the twin dislocations of this Lehmann cluster separate one from the other and tend to adopt the circular shape of radius $r_{0,1}$ as shown in Figure 7b.

View Article Online
DOI: 10.1039/D5SM01244A

2.6 Peach-Koehler force

This behavior is determined by the dependence of the Peach-Koehler force on the local thickness h. This force per unit length corresponds to the difference between the densities of the distortion energy per unit area on the two sides of the twin dislocations. On the side with $N=0$ one has

$$f_0 = h\frac{K_{22}}{2}\left(\frac{2\pi}{p_o}\right)^2 \quad (1)$$

(K_{22} is the twist elastic coefficient) while on the other side with $N=1$ one has

$$f_1 = h\frac{K_{22}}{2}\left(\frac{2\pi}{h}-\frac{2\pi}{p_o}\right)^2 = h\frac{K_{22}}{2}\left(\frac{2\pi}{p_o}\right)^2\left(\frac{p_o}{h}-1\right)^2 \quad (2)$$

The Peach-Koehler is thus

$$F_{PK} = f_1 - f_0 = p_o\frac{K_{22}}{2}\left(\frac{2\pi}{p_o}\right)^2\left(\frac{p_o}{h}-2\right) \quad (3)$$

It changes sign for $h = p_o/2$.

In the cylinder/cylinder geometry, where the thickness h varies with the distance r from the gap center as

$$h(r) \approx h_{min} + \frac{r^2}{2R} \quad (4)$$

the sign of the Peach-Koehler force changes on the circle of radius

$$r_{0,1} \approx \sqrt{2R(p_o/2 - h_{min})} \quad (5)$$

which is drawn with a dashed line in Figure 7b.

For $r > r_{0,1}$, the Peach-Koehler force pushes the twin dislocations one against the other and the Lehmann cluster is stable.

For $r < r_{0,1}$, the Lehman cluster splits and the two twin dislocations tend to take semi-circular shapes of radius $r_{0,1}$ for which the Peach-Koehler force vanishes.

Deviations from these ideal linear and circular shapes are due to the Laplace force given by

$$F_{Lap} = \frac{T_{0,1}}{\rho} \quad (6)$$

where $T_{0,1}$ is the tension of dislocations and ρ the radius of their local curvature. Their discussion is out of the scope of this paper.

3 Topological immunity of Lehmann clusters against annihilation

As we will see below, the topological immunity against annihilation of the dislocations pairs forming Lehmann clusters is related to the singularity-free director fields of the individual dislocations themselves. Such singularity-free fields can be constructed by the geometrical method illustrated by Figure 8 and discussed in details in Section 1.1 of Supplementary Information, where it is applied to the simplest case of a $b = p$ dislocation separating fields with $N=1$ and $N=0$ cholesteric pitches as discussed above (see Figure 6).

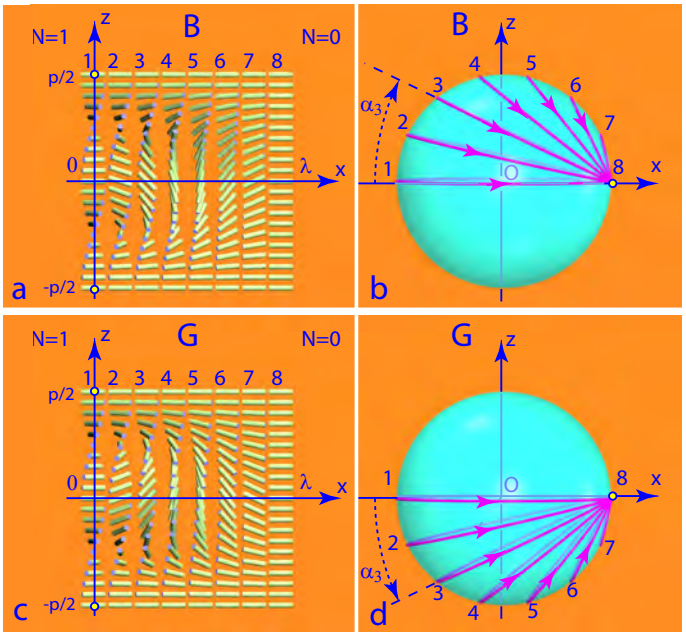

Figure 8 Two variants, B and G, of a singularity-free director field of the dislocations with the Burgers vector $b = p$. a and c) Director field. b and d) Mapping of the director field on the unit sphere. The two variants are related by rotation by π around the x axis.

3.1 B variant of the singularity-free director field of dislocations with the Burgers vector $b = p$

Let us consider first the field $\mathbf{n}_B(x,z)$ in Figure 8a labeled as "B". **It can be seen as a wall of width λ across which the cholesteric helix $\mathbf{n}(0,z) = (\cos(2\pi z/p), \sin(2\pi z/p), 0)$, depicted in column 1, is deformed continuously into the homogeneous field $\mathbf{n}(\lambda,z) = (1,0,0)$ depicted in column 8.**

When the field $\mathbf{n}_B(x,z)$ is mapped onto the unit sphere in Figure 8b, the whole north hemisphere is covered. In particular, the column 1 with $\mathbf{n}_B(0,z) = (\cos(2\pi z/p), \sin(2\pi z/p), 0)$ is mapped onto the equator. When one moves from z=-p/2 to z=p/2 in this column 1, the director field starts from the orientation $\mathbf{n}_B(0,-p/2) = (1,0,0)$ represented by the yellow dot (imposed by the anchoring on the lower mica sheet) and rotates by the azimuthal angle 2π around the z-axis until it returns to the the orientation $\mathbf{n}_B(0,p/2) = (1,0,0)$ imposed by the anchoring on the upper mica sheet. By this means, the column 1 is mapped onto the equator.

The column 8 with $\mathbf{n}_B(\lambda,z) = (1,0,0)$ is mapped as a whole onto the yellow dot.

The intermediate columns labeled as $i = 2,...,7$ are mapped successively on circles making angles $\alpha_i = (i-1)\pi/14$ with the equator and passing through the yellow dot $(1,0,0)$.

The analytical expression of the director field of the B variant is given in Section 1.1 of Supplementary Information.

3.2 G variant of the singularity-free director field of dislocations with the Burgers vector $b = p$

The director field $\mathbf{n}_G(x,z)$ of the second, G variant of the singularity-free director field of dislocations with the Burgers vec-

View Article Online
DOI: 10.1039/D5SM01244A

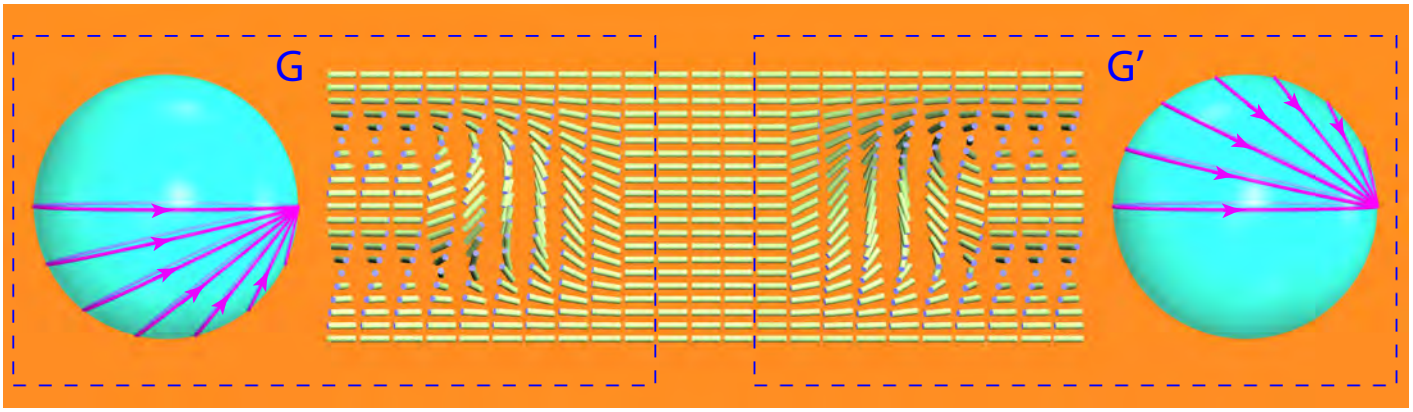

Figure 9 Construction of the Lehmann cluster from two G-type singularity-free dislocations defined in Figure 8. The director field of the dislocation G' is obtained from dislocation G by rotation as a whole by π around the z-axis. Director fields of the two dislocations are matched by a band of a uniform field $\mathbf{n} = (1,0,0)$.

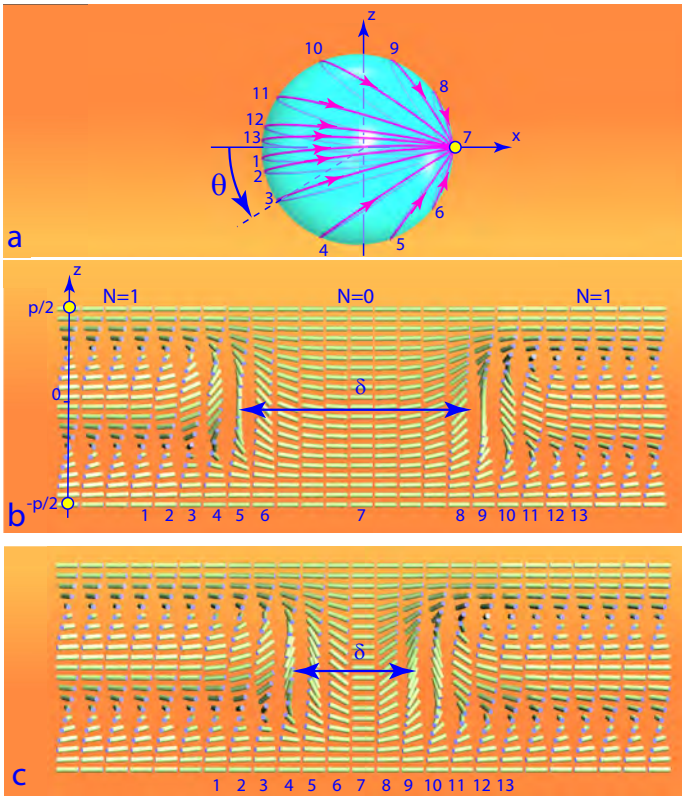

Figure 10 Immunity against annihilation of the GG' dislocation pair defined in Figure 9. a) Mapping on the unit sphere of director fields shown in (b) and (c). No matter what is the distance δ between the dislocations, the whole unit sphere is covered completely because the angle θ varies always from 0 to 2π. For this reason the GG' pair of dislocations is immune against annihilation.

tor $b = p$ is represented graphically in Figs. 8c. It is related to the variant B by rotation of the field $\mathbf{n}_B(x,z)$ as a whole by π around the x-axis.

When mapped on the unit sphere, the field $\mathbf{n}_G(x,z)$ covers the whole south hemisphere. Its columns, labeled $i = 1,...,8$, are mapped on circles making angles $\alpha_i = -(i-1)\pi/14$ with the x axis.

3.3 GG and BB dislocation pairs are immune against annihilation

Dislocations of the G- and B-types can form four types of pairs: GG, BB, GB and BG.

The director field of the GG pair is depicted in Figure 9. Here, the dislocation on the right labeled as G' is of the G-type. It is related to the dislocation G on the left by rotation by π around the z axis. The space between the G and G' dislocations is filled by the uniform field $(1,0,0)$.

Figure 10 shows that the mapping of the director field of the GG' pair covers completely the unit sphere **independently of the distance δ between dislocations**. For this topological reason, the GG' pair is immune against annihilation.

The same conclusion is reached in the case of the BB pair.

3.4 GB and BG pairs are subjected to annihilation

The director field of the GB pair is depicted in Figure 11. Here, the dislocation on the right labeled as B' is of the B-type. It is related to the dislocation B defined in Figure 8b by rotation by π around the z axis. The space between the G and B' dislocations is filled by the uniform field $(1,0,0)$.

Figure 12 shows that the mapping of the director field of the GB' pair covers only partially the south hemisphere. The area Σ covered by the mapping decreases with the distance δ between dislocations. In the limit $\Sigma \to 0$, the annihilation occurs. The same conclusion is reached in the case of the BG pair.

We can conclude that stable GB and BG pairs of dislocations should not exist which actually is confirmed by our experiments.

View Article Online
DOI: 10.1039/D5SM01244A

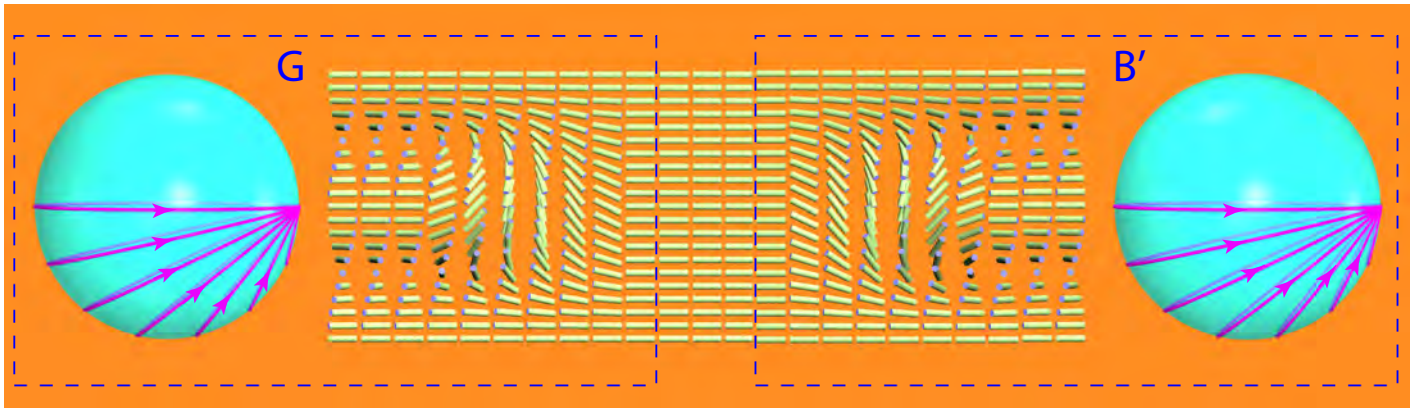

Figure 11 Pair of the G-type and B-type singularity-free dislocations defined in Figure 8. The director field of the dislocation B' is rotated as a whole around the z-axis by π with respect to the dislocation B. Director fields of the two dislocations are matched by a band of a uniform field $\mathbf{n} = (1,0,0)$.

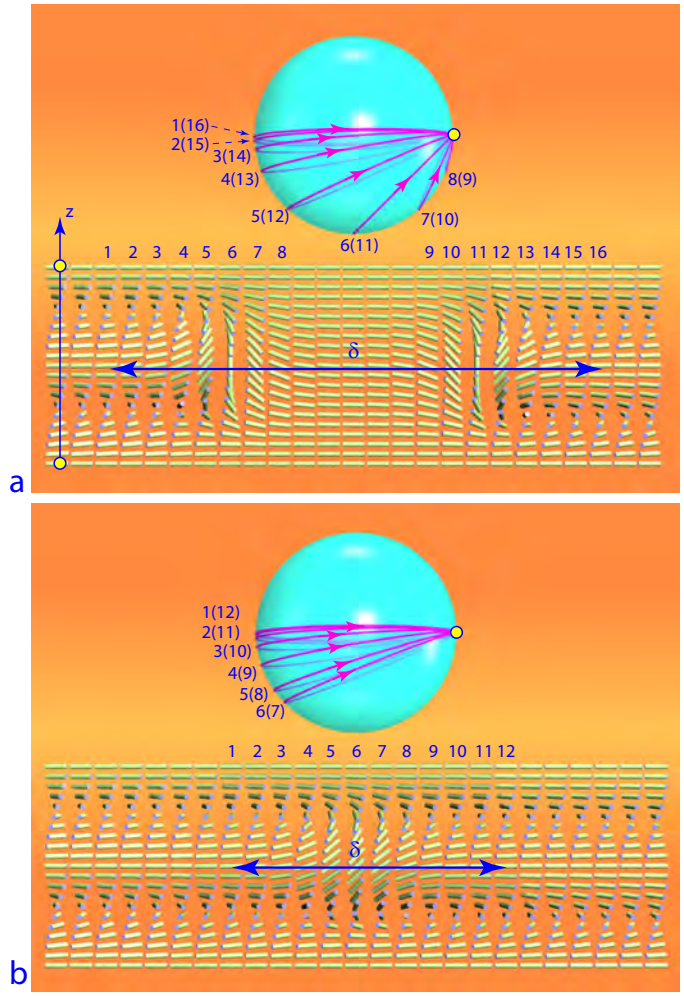

Figure 12 Singularity-free director field of the dislocation pair GB' defined in Figure 11 is subjected to annihilation. a) Mapping of the director field on the unit sphere for a large distance δ between dislocations. Only the south hemisphere is covered by the mapping. b) When the distance δ decreases, the surface Σ covered by the mapping shrinks. In the limit $\Sigma \to 0$, the annihilation occurs. For this reason, stable pairs of the GB' type have not been observed in experiments.

4 Structure and energy of Lehmann clusters

4.1 Orientation of Lehmann clusters

In the previous section we have assumed arbitrarily that dislocations forming Lehmann clusters inside the $N = 1$ annular field are orthogonal to the anchoring direction. Now, experiment reported in Section 2.3 (see Figures 5b-d) shows that the Lehmann clusters can have arbitrary orientations. It is therefore necessary to ask how the director field of a Lehmann cluster depends on its orientation defined in Figure 13a, i.e., on the angle γ that it makes with the direction of the anchoring which is assumed to be the same on both mica sheets.

4.2 Dependence of the structure on the orientation angle γ

For the sake of simplicity let us consider again the case of Lehmann clusters inside the $N = 1$ field.

The case of the Lehmann cluster orthogonal to the anchoring direction corresponds to $\gamma = \pi/2$ (see Figure 13a) and its director field, represented in the first column and the second row of Figure 13c, is the same as the one in Figure 10c.

Starting from this director field $\mathbf{n}_{\pi/2}(\xi, z)$, it is easy to obtain fields $\mathbf{n}_\gamma(\xi, z)$, corresponding to other values of the angle γ, by a simple geometrical transformation: a rotation of the director by the angle $\psi = \gamma - \pi/2$ around local vertical axes ζ_ξ (parallel to z) passing through the point ξ on the horizontal axis ξ. For $\psi < 0$ and $\psi > 0$, rotations are respectively in anticlockwise and clockwise directions.

In Figure 13c, we represent the set of eight fields, obtained by this method, corresponding to $\gamma = 0, \pi/4, 2\pi/4, ..., 7\pi/4$.

4.3 Energy versus the orientation angle γ: theory

All eight configurations of the director field $\mathbf{n}_\gamma(\xi, z)$ have right-hand twist distortions in the z direction.

There is also a twist distortion in the horizontal ξ direction but its sign and amplitude depends on the angle γ. As shown in Figure 13c, in the field $\mathbf{n}_0(\xi, z)$, the twist is right-handed, i.e. the same as in the z direction, while in the field $\mathbf{n}_\pi(\xi, z)$, the twist distortion has opposite handedness. For this reason, the energy per unit length of Lehmann clusters $E_{LC}(\gamma)$ in the configuration

View Article Online
DOI: 10.1039/D5SM01244A

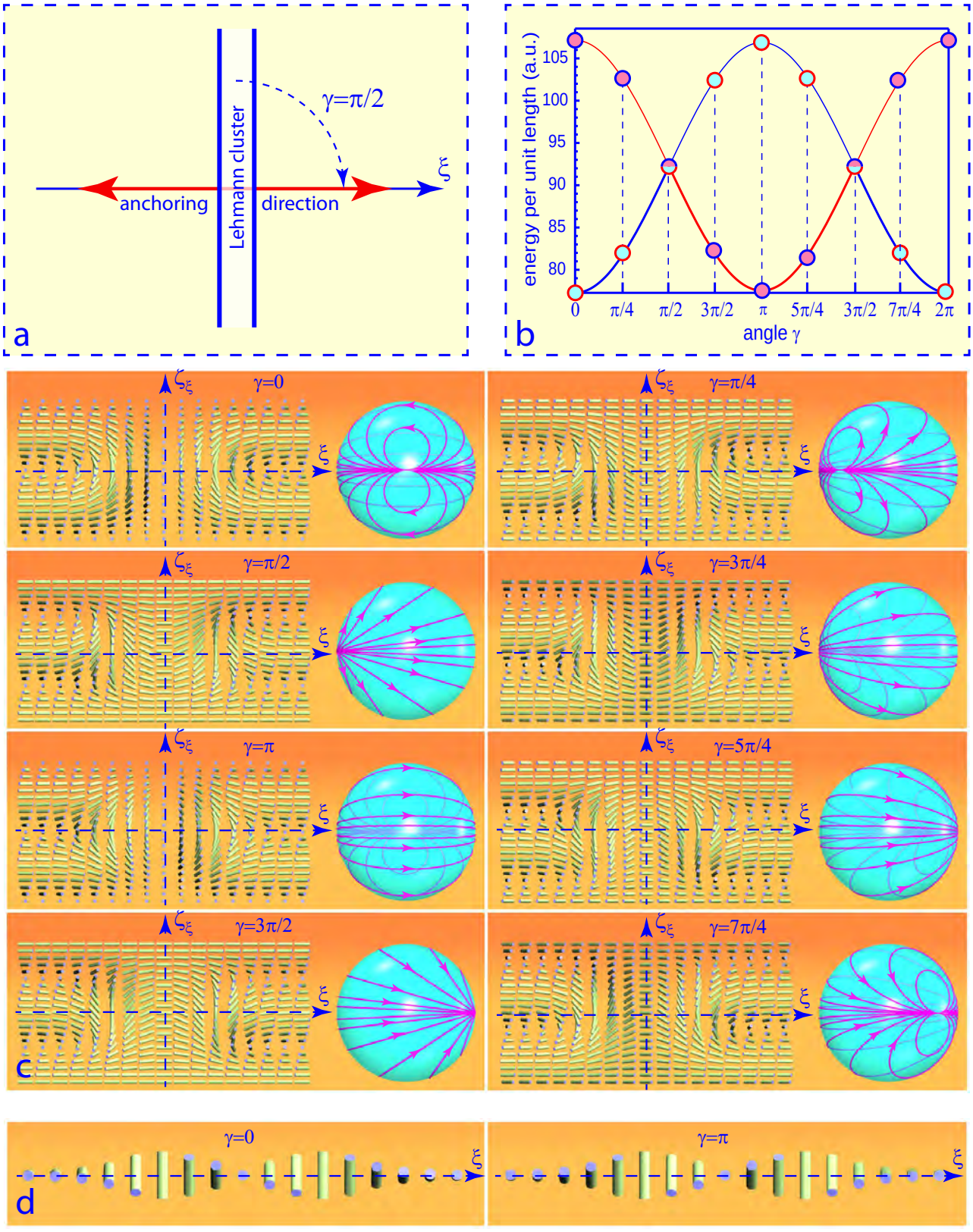

Figure 13 Dependence of the structure and energy of Lehmann clusters on their orientation with respect to the anchoring. a) Definition of the angle γ between a Lehmann cluster and the anchoring direction. b) Variation of the energy with the orientation angle γ. c) Dependence of the director field of Lehmann clusters on their orientation angle γ. d) Twist distortions along the horizontal axis ξ for $\gamma = 0$ and $\gamma = \pi$.

View Article Online
DOI: 10.1039/D5SM01244A

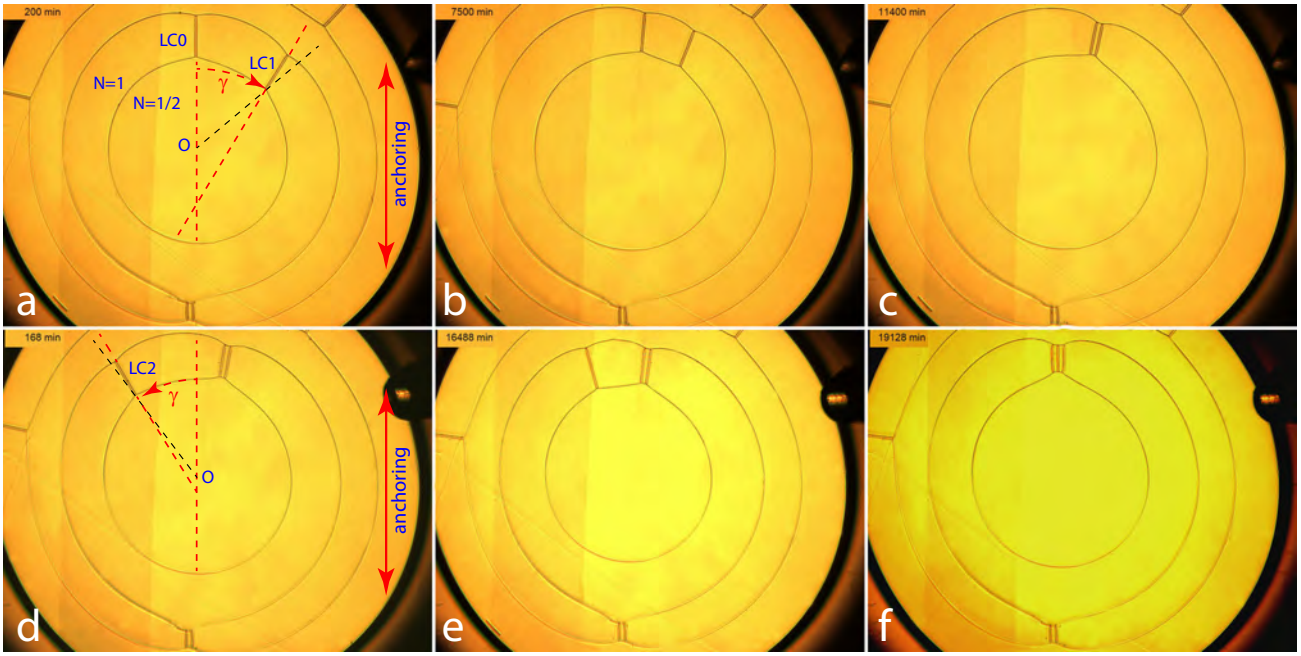

Figure 14 Evolution of the orientation of Lehmann clusters. The orientation of the Lehman cluster LC0 parallel to the anchoring corresponds to the minimum of its energy. a) Shortly after its generation, the new Lehmann cluster LC1 is not orthogonal to the adjacent $p/2$ concentric dislocation loops because there is an elastic torque acting on it due to the torque $\Gamma = \partial T/\partial\gamma$. b-c) The subsequent orthoradial drift of the Lehmann cluster LC1 toward LCO reduces its length and tension $T(\gamma)$. d-f) The same behavior is observed with the Lehmann cluster LC2. Note that the final collision between Lehmann clusters does not result in annihilation. (see Videos 2 and 3 of Supplementary Information)

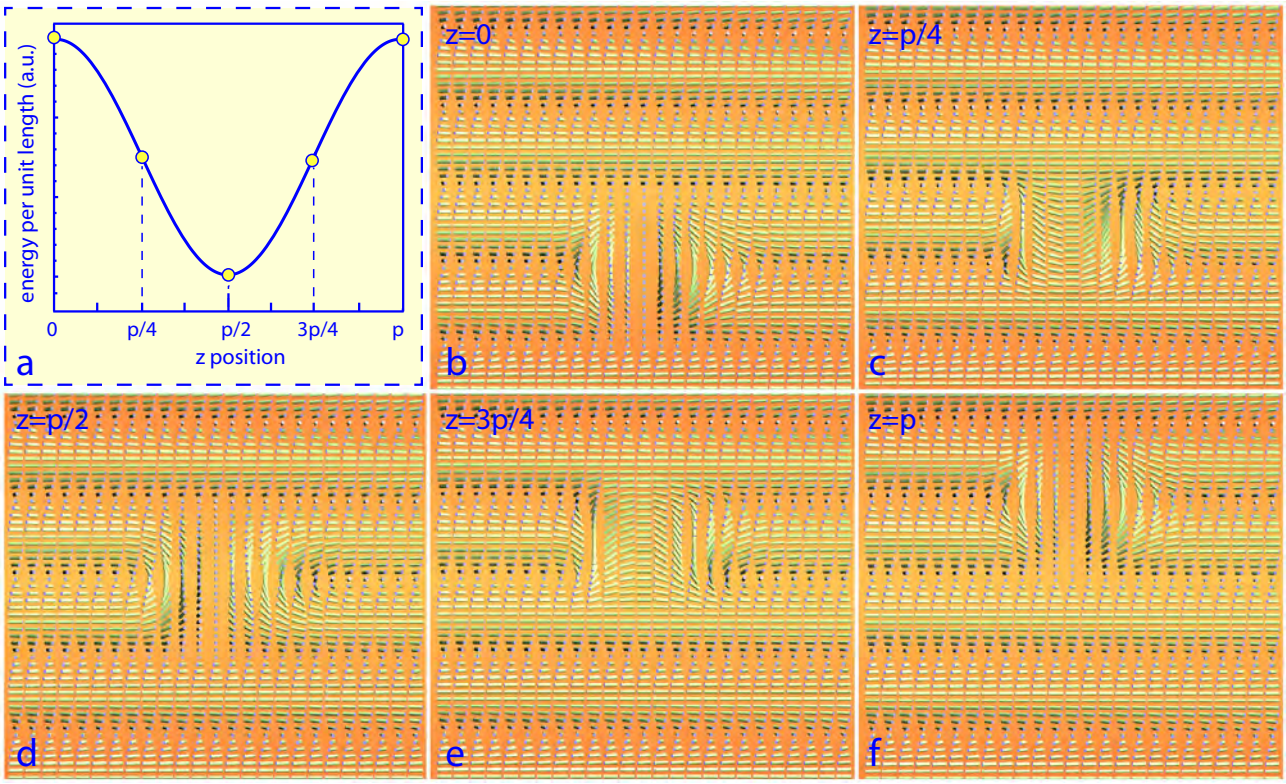

Figure 15 Dependence of the structure and energy of Lehmann clusters on their z position inside a sample of thickness "N=2.5". a) Dependence of the energy of Lehmann clusters on their z position. b-f) Dependence of the structure of Lehmann clusters on their z position.

View Article Online
DOI: 10.1039/D5SM01244A

labeled $\gamma = 0$ shown of Figure 13c (first column, first row) is expected to be lower than that of the configuration $\gamma = \pi$ (first column, third row).

Numerical calculation of the energy $E_{LC}(\gamma)$ of the configurations shown in Figure 13c (see Supplementary Information Section 1.2) confirms this expectation: the red line plot of $E_{LC}(\gamma)$ in Figure 13b has a minimum for $\gamma = 0$ and a maximum for $\gamma = \pi$.

Let us stress that in the diagram of Figure 13b, there is a second plot drawn with a blue line which is obtained by shifting the red line by π. Its presence is required by symmetry : as the anchoring direction is represented in Figure 13a by a two headed arrow, the angle γ is equivalent to $\gamma + \pi$. Therefore, for each value of γ, two configurations of the director field with different energies $E_{LC}(\gamma)$ and $E_{LC}(\gamma + \pi)$ are possible. In Figure 13b, plots with thick red and blue lines correspond to configurations with lower energies.

4.4 Energy versus the orientation angle γ: experiments

The dependence of the energy of Lehmann clusters T on their orientation γ with respect to the anchoring has been detected in experiments performed with a cylinder/cylinder wedge of minimal thickness $h_{min} < p/2$. In Figure 14, we show changes in the direction of Lehmann clusters driven by the torque $\Gamma = \partial T/\partial\gamma$.

Let us consider, for example, the behavior of the Lehmann cluster LC1 in Figures 14a-c. Shortly after its generation by the $cholesteric \rightarrow isotropic \rightarrow cholesteric$ phase sequence, the Lehmann cluster LC1 is not orthogonal to the adjacent $p/2$ concentric dislocation loops because the elastic torque $\Gamma = \partial T/\partial\gamma$ is acting on. On a longer time scale, the Lehmann cluster slowly drifts toward the orientation parallel to the anchoring direction corresponding to the minimum of the tension $T(\gamma)$.

The Lehmann cluster LC2 generated subsequently has the same behavior: it drift also toward the orientation of the anchoring (see Figures 14d-f) (see Video 2 of Supplementary Information).

By these two generation-drift processes, a stable set of three Lehmann clusters gathered together is visible in Figure 14f. In section 5 we will explain why, in this set, the Lehmann clusters are protected against annihilation.

4.5 Energy and structure versus the z position

Above, for the sake of simplicity, we considered Lehmann clusters embedded in the field $N = 1$. In practice, as shown in Figure 15, Lehmann clusters can be embedded also in a thicker field, for example, $N = 5/2$. In this case, the structure and the energy per unit length T of a Lehmann cluster depend not only on its orientation but also on the level z inside the sample. When the orientation of the Lehmann cluster is given by the azimuthal angle γ and its position inside the stack by the coordinate z, then its energy T depends, in principle, on both variables : $T = T(\gamma, z)$. However, the energy T should be invariant with respect to the operations of the screw symmetry axis of the cholesteric helix. This requirement is satisfied when the tension T depends only on the linear combination $\psi = \gamma - 2\pi z/p$ where p is the local pitch of the cholesteric helix:

$$T = T(\gamma - 2\pi z/p) \tag{7}$$

5 Larger sets of dislocation topologically protected against annihilation

5.1 Gathering together of Lehmann clusters

In the experiment depicted in Figure 5, new Lehmann clusters have been generated inside the $N = 1$ field by local cholesteric $\rightarrow$ isotropic $\rightarrow$ cholesteric phase transitions. Experiments show that Lehmann clusters generated by this method inside the same annular field labeled N between two adjacent $b = p/2$ dislocations have tendency to gather together due to an attractive interaction involving their own tension as well as the tensions of the $b = p/2$ dislocations.

For example, in Figs. 5b-d, two Lehmann clusters are gathered together inside the N=3/2 annular field, while in Figure 16a three Lehmann clusters are gathered together inside the N=1 field.

5.2 Immunity against annihilation of colliding Lehmann clusters

We will point now that stability of sets of several Lehmann clusters gathered together is of the same topological nature as the stability of the individual Lehmann clusters made of two dislocations with opposite Burgers vectors $b = p$ and $b = -p$.

5.3 Models of the director field of the set of three Lehmann clusters

For this purpose let us consider models of the director field inside cross sections (ξ, z) defined in Figure 16a. In Figure 16c we show four models corresponding to different orientations of the three Lehmann clusters with respect to the anchoring direction defined in Figure 16b.

When the Lehmann clusters are orthogonal to the anchoring direction, their director field has structures depicted in the first and third rows of Figure 16c labeled as GG' or BB' previously. In these two cases, the director at the mid-height of the sample (z=0) stays in the plane (ξ_1, z) or (ξ_3, z) and rotates by the angle θ in anticlockwise or clockwise direction as already discussed above.

On the other hand, when Lehmann clusters are parallel to the anchoring direction, their director field has structures depicted in the second and fourth rows of Figure 16e. Here, the director at the mid-height of the sample (z=0) is orthogonal respectively to the ξ_2 and ξ_4 axes and rotates by the angle θ around them in anticlockwise or clockwise directions.

A model of the director field of this set of three Lehmann clusters in the (ξ_1, z) cross section defined in in Figure 16a is shown in Figure 16d. When mapped on the unit sphere in Figure 16e, it covers it three times. For $z = 0$, the director rotates by $\theta(\xi_1)$ in the (ξ_1, z) plane and can be expressed as

$$\mathbf{n}(x, 0, 0) = [\cos\theta(x), 0, \sin\theta(x)] \tag{8}$$

View Article Online
DOI: 10.1039/D5SM01244A

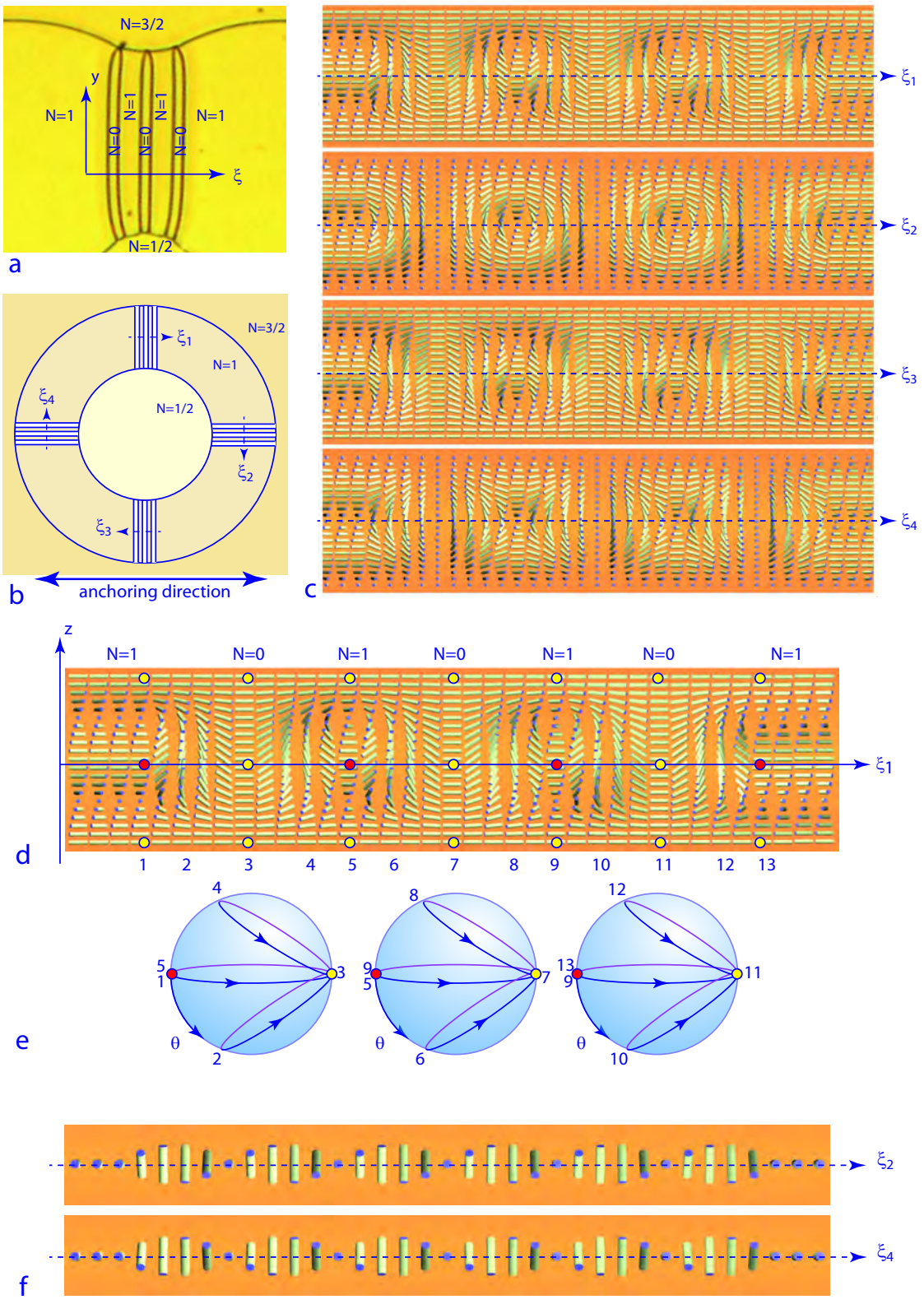

Figure 16 Topologically protected sets of three Lehmann clusters. a) View in a microscope. b) Four different orientations of Lehmann clusters with respect to the anchoring direction. c) Director fields corresponding to the four orientations defined in (b). d) Singularity-free model of the director field in the (ξ_1, z) cross section along the ξ_1-axis, defined in (a), which is parallel to the anchoring direction on mica surfaces. e) The mapping of the director field onto the unit sphere covers it three times. f) The director field at mid-height z=0 along the ξ_2-axis forms a right-hand helix while along the ξ_4-axis the helix is levogyre.

View Article Online
DOI: 10.1039/D5SM01244A

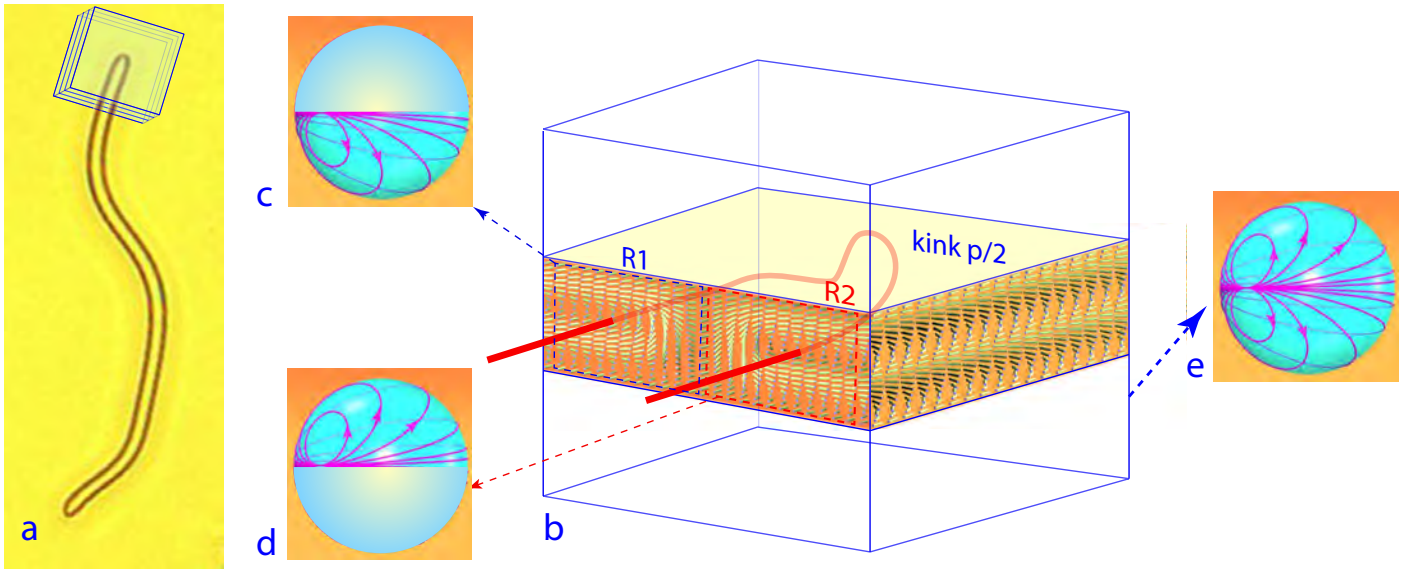

Figure 17 Monopoles located at extremities of a skyrmion tube of finite length. a) Lehmann cluster of finite length observed in experiments (see Figure 4d). It is equivalent to a skyrmion tube. One of its extremities is located inside a cuboid box. b) Director field on surfaces of the cuboid. c) Director field from the rectangle R1 covers the south hemisphere. d) Director field from the rectangle R2 covers the north hemisphere. d) Director field from the surface of the whole cuboid covers the whole unit sphere. Note the presence of a $p/2$ kink on the U-turn of the dislocation forming the skyrmion tube (Lehmann cluster).

where the function $\theta(\xi_1)$ is monotonically growing from 0 to 6π. Figure 16f shows that the director fields $n(\xi_2, 0)$ and $n(\xi_4, 0)$ form respectively right-hand and left-hand helices. As in the mixtures of 5CB with CB15 the cholesteric helix is dextrogyre, the structure of the Lehmann clusters depicted in the second row of Figure 16e has the lowest energy.

6 Skyrmionic topology perspective

It is instructive to analyze the structures discussed above from the perspective of topological solitons like skyrmion and fractional skyrmion tubes [10,11]. This analysis can also help connecting the fundamental aspects of our findings in liquid crystals to that in other physical systems, like colloidal and solid-state magnets and optics [10–18].

6.1 Vectorization of the nonpolar director's order parameter

The director fields of nonsingular solitonic structures corresponding to b=p quasi-layer dislocations that we study here can be smoothly vectorized by decorating the rod-like molecules with unit vectors of different orientations in three dimensions [19]. Such vectorization converts the nonpolar director's order parameter space of S^2/Z_2 into S^2. This is possible because all two-dimensional (and ones with higher dimensionality) topological soliton objects can be smoothly vectorized without creating any extra singularities [10]. The process of decorating the nematic director field lines with vectors has the actual physical implementation in molecular-colloidal chiral liquid crystal systems where magnetically monodomain colloidal particles can be doped into the nonpolar molecular nematic host medium, so that unit vectors due to magnetic moments of the nanoplates align in one of the two non-distinguishable orientations of the director with nonpolar symmetry [13]. The finite-length fragments of Lehman clusters (skyrmion tubes) in a bulk of chiral nematic are known terminating on point defects [11], which, similar to skyrmion tubes themeselves, can be also smoothly vectorized.

6.2 Equivalence between the Lehmann clusters and skyrmion tubes

From the homotopy theory, $\pi_2(S^2) = Z$ [10,20]. Therefore, topologically stable skyrmion tubes are allowed and expected in chiral nematics, similar to a host of other media in which such configurations are studied recently [11,17]. In fact, Lehman clusters have been previously identified as such objects in both nonpolar molecular and ferromagnetic colloidal chiral liquid crystals [13,20].

Since the homotopy theory description of skyrmion tubes and singular point defects in 3D is similar, $\pi_2(S^2) = Z$ [10,19,21,22], it is natural that the fragments of the skyrmion tubes would terminate at the the topological objects with monopole topology of the same homotopy class $\pi_2(S^2) = Z$ [11], which can be found in the micrographs shown in Fig. 4d and in Fig. 17

6.3 Equivalence between b=p dislocations and merons

Each of the interacting nonsigular quasi-layer dislocations can be interpreted as a meron (also often referred to as "half-skyrmion") [11,15,16]. Depending on the relative signs of the fractional skyrmions numbers of merons, they can either annihilate (for the case of opposite signs) or combine into a composite topological soliton with an integer-valued skyrmion number [18]. We note that the relative signs of the skyrmion numbers can be determined upon smooth vectorization of the director field, though

View Article Online
DOI: 10.1039/D5SM01244A

the procedure of mapping the director field patterns onto the two-sphere that we use is equivalent to it because S^2 is the order parameter space for the unit vector field in 3D.

6.4 Skyrmions and merons embedded into helical background

The skyrmions and merons embedded into helical background have been explored extensively in chiral non-centrosymmetric magnets and light fields[15,16,23], in magnetic colloidal liquid crystals[13], as well as other research fields where they often have structures vividly similar to the quasi-layer dislocations and Lehman clusters in chiral nematic liquid crystals[6,10,15,16,24]. From the skyrmionic topology perspective, the three Lehman clusters shown in Figure 3a are skyrmion tubes of the same elementary skyrmion number, each composed of pairs of merons in the form of inter-bonded quasi-layer dislocations of B-B or G-G type in the helicoidal director field, interacting with each other repulsively. In addition to the prevalent case of the two merons (dislocations) being located at the same depth level, situations can arise when the dislocations would be localized at different levels of quasi-layered system of the chiral nematic medium (see such an example in Fig. 15a and b in ref. [1]). In this case, additional energetic stability can be endowed to the dislocations (merons) by the need of continuity of helical quasi-layers that separate them.

6.5 Chiral nematics as a playground of merons and skyrmions: fundamentals and utility

The high experimental accessibility of chiral nematic liquid crystals allows us to see in great detail the processes of annihilation and hybridization of merons that in the end form topologically stable skyrmion tubes. While the structures we depict are shown in a highly simplified schematic forms, which allow us to directly convey the implications of mappings from physical configurational space to order parameter space in terms of topological protection and stability, we note that geometrically different but topologically the same configurations can be observed when the axes of the skyrmion or meron tubes are smoothly translated across the depth of the sample (helical axis).

The topological and energetic stability of such structures may allow for their technological utility in applications like guiding beams of light[25–27]. In the past, structures of optical axis associated with various defects and topological solitons were utilized in controlling light mainly in non-chiral nematic media whereas the opportunities that can be potentially presented by the chiral nematic topological solitons have been largely overlooked despite the fact that they would be capable of guiding and steering laser light[26,27], calling for future research in this direction

7 Conclusions and outlook

The very good experimental accessibility of liquid crystalline topological structures allowed us to explore the nature of non-singular quasi-layer dislocations and their interactions when embedded within the chiral nematic's helical background, demonstrating how Lehman clusters and b=p dislocations can be understood as translationally invariant skyrmion and meron tubes. We demonstrated that the stability of these objects is enhanced by the phenomenon known in the liquid crystal field as the "escape into the third dimension" of the director field, effectively endowing the chiral topological soliton nature to these structures. We showed that, from a topological point of view, the Lehmann clusters can be interpreted as skyrmion tubes, with topologically-monopole-like structures at their extremities in the case of their finite length. Our findings may provide vivid insights into solitonic-topology-enriched physical behavior that could have analogues in other research fields, like magnetism and optics and pure mathematics[12,15,17,27–33], as well as could have technological utility ranging from waveguiding laser light[26–28] to the control of surface topography in cholesteric elastomers. The study of similar objects in magnets has the potential for enabling various new types of data storage[15], where our work presented here could serve as an inspiration.

Conflicts of interest

There are no conflicts to declare.

Data Availability Statement

The data supporting this article have been included as part of the SI. The supplementary information file contains the list of the videos quoted in the article. See DOI: .....

Acknowledgements

P.P., I.S. and M.H.G. thank the organizers of the ECLC 2025 conference for the invitation. The experimental setup tailored for production of the cholesteric dislocations in the cylinder/ cylinder mica wedges was built by V. Klein, J. Sanchez, and S. Saranga. I.I.S. acknowledges the support by the U.S. Department of Energy, Office of Basic Energy Sciences, Division of Materials Sciences and Engineering, under contract DE-SC0019293 with the University of Colorado at Boulder. I.I.S. and P.P. acknowledge the support of the International Institute for Sustainability with Knotted Chiral Meta Matter (WPI-SKCM2), and international institute of Japan's World Premier Initiative, which facilitated and supported their collaboration. This work has been supported by the ERC H2020 Synergy grant 101167171 (ALCEMIST). We have greatly benefited from discussions with Y. Pomeau, P. Oswald, O. Lavrentovich, A. Leforestier and C. Goldmann, as well as from the help of S. Assimomitis, J. Saen, Y. Simon, M. Bottineau, B. Senyuk, J.-S. Wu and I. Nimaga. M.H.G. acknowledges a financial support from Foundation for Science and Technology 2022.04191.PTDC (ColorSafe).

Notes and references

1 I. Smalyukh and O. Lavrentovich, *Phys. Rev. E*, 2002, **66**, 051703.
2 M. Kleman and J. Friedel, *Le Journal de Physique Colloques*, 1969, **30**, C4–43.
3 B. A. Wood and E. L. Thomas, *Nature*, 1986, **324**, 655–657.
4 S. D. Hudson and E. L. Thomas, *Physical Review A*, 1991, **44**, 8128.
5 P. Pieranski, M. Zeghal, M. H. Godinho, P. Judeinstein,

View Article Online
DOI: 10.1039/D5SM01244A

R. Bouffet-Klein, B. Liagre and N. Rouger, *Physical Review Letters*, 2023, **131**, 128101.
6 P. Pieranski and M. Godinho, *Liquid Crystals*, 2024, **51**, 2144–2175.
7 P. Pieranski and M. H. Godinho, *Comptes Rendus. Physique*, 2024, **25**, 367–388.
8 J.-Y. Lee, M. Zeghal, P. Judeinstein, M. H. Godinho, I. Smalyukh and P. Pieranski, *Soft Matter*, 2025, **21**, 8205–8218.
9 P. Pieranski, *Liquid Crystals Reviews*, 2022, **10**, 3–33.
10 I. I. Smalyukh, *Reports on Progress in Physics*, 2020, **83**, 106601.
11 J.-S. Wu and I. I. Smalyukh, *Liquid Crystals Reviews*, 2022, **10**, 34–68.
12 N. Nagaosa and Y. Tokura, *Nat. Nanotechnol.*, 2013, **8**, 899—911.
13 Q. Zhang, P. J. Ackerman, Q. Liu and I. I. Smalyukh, *Phys. Rev. Lett.*, 2015, **115**, 097802.
14 R. D. Kamien and R. A. Mosna, *New Journal of Physics*, 2016, **18**, 053012.
15 A. Fert, N. Reyren and V. Cros, *Nature Reviews Materials*, 2017, **2**, 1–15.
16 H. Kedia, I. Bialynicki-Birula, D. Peralta-Salas and W. T. Irvine, *Physical Review Letters*, 2013, **111**, 150404.
17 B. Wang, Z. Che, C. Cheng, C. Tong, L. Shi, Y. Shen, K. Y. Bliokh and J. Zi, *Nature*, 2025, **638**, 394–400.
18 J.-S. B. Tai, A. J. Hess, J.-S. Wu and I. I. Smalyukh, *Science advances*, 2025, **10**, eadj9373.
19 P. J. Ackerman, R. P. Trivedi, B. Senyuk, J. van de Lagemaat and I. I. Smalyukh, *Physical Review E*, 2014, **90**, 012505.
20 R. Voinescu, J.-S. B. Tai and I. I. Smalyukh, *Phys. Rev. Lett.*, 2020, **125**, 057201.
21 G. Toulouse and M. Kleman, *Journal de Physique Lettres*, 1976, **37**, L–149.
22 G. Toulouse, "*Sens d'une exploration*" *dans Le goût de la science*, Alvik, Paris, 1st edn., 2005.
23 M. Berry and M. Dennis, *Proc. R. Soc.*, 2001, **111**, 2251–2263.
24 J.-S. B. Tai, P. J. Ackerman and I. I. Smalyukh, *PROC. NATL. ACAD. SCI. U.S.A.*, 2018, **115**, 921–926.
25 C. Meng, J.-S. Wu and I. I. Smalyukh, *Nature Materials*, 2023, **22**, 64–72.
26 G. Poy and S. Žumer, *Optics Express*, 2020, **28**, 24327.
27 G. Poy, A. J. Hess, I. I. Smalyukh and S. Žumer, *Physical Review Letters*, 2020, **125**, 077801.
28 A. J. Hess, G. Poy, J.-S. B. Tai and S. Žumer, *Phys. Rev. X*, 2020, **10**, 031042.
29 U. Tkalec, M. Ravnik, S. Čopar, S. Žumer and I. Muševič, *Science*, 2011, **333**, 62–65.
30 L. H. Kauffman and S. Lambropoulou, *Advances in Applied Mathematics*, 2004, **33**, 199–237.
31 P. Pieranski and M. H. Godinho, *The European Physical Journal Special Topics*, 2024, 1–21.
32 B. Zappone and R. Bartolino, *Proceedings of the National Academy of Sciences*, 2021, **118**, e2110503118.
33 L. H. Kauffman and S. Lambropoulou, in *Topology in Molecular Biology*, Springer, 2007, pp. 69–110.

View Article Online
DOI: 10.1039/D5SM01244A

Data Availability Statement

The data supporting this article have been included as part of the SI. The supplementary information file contains the list of the videos quoted in the article. See DOI: …….